



## Short communication

## About internal currents during start-up in proton exchange membrane fuel cell

Gael Maranzana\*, Christian Moyne, Jerome Dillet, Sophie Didierjean, Olivier Lottin

LEMMA, Nancy-University, CNRS 2, Avenue de la forêt de Haye, B.P. 160, 54504 Vandoeuvre-les-Nancy Cedex, France

## ARTICLE INFO

## Article history:

Received 30 September 2009

Received in revised form 29 October 2009

Accepted 29 October 2009

Available online 6 November 2009

## Keywords:

Fuel cell  
Reverse current  
Internal current  
Start-up

## ABSTRACT

This paper reports about an experimental and numerical study of the internal currents that occur during fuel cell start-up under open-circuit conditions. The internal currents were measured in a segmented cell specifically designed for this purpose and it was found that they could reach values higher than  $1 \text{ A cm}^{-2}$ . They result from the potential that appears at the inlet of the anode compartment while hydrogen pushes oxygen, air, or possibly nitrogen that was introduced for purging water toward the outlet. For a short time, a fraction of the channels is filled with hydrogen while the other part is still occupied by the gas initially present. The model presented in the paper demonstrates that the occurrence of internal currents can be explained mostly by capacitive effects. Carbon oxidation occurs probably simultaneously but its contribution to the internal currents is by all appearances negligible. The model also explains the transient voltage rise (over the steady state open circuit voltage) that is sometimes observed experimentally shortly after the fuel cell start-up.

© 2009 Elsevier B.V. All rights reserved.

## 1. Introduction

As proton exchange membrane fuel cells (PEMFC) begin to come on to the market, the reliability and lifespan of their membrane electrode assemblies (MEAs) remains a major problem. Their degradation mechanisms are not yet well understood, although several working conditions are known to be damaging [1]. For instance, supplying the fuel cell with dry gases can induce a fast degradation of the electrodes [2] but on the other hand, long-time or repeated storage without purging liquid water from the gas channels accelerates the fuel cell aging [3]. Potential cycling [4] or operation under open-circuit conditions [5] are also to be avoided. This paper reports about an experimental and numerical study of the internal currents that occur during fuel cell start-up under open-circuit conditions. Shut-down/start-up cycling results in performance degradation according to Tang et al., Shen et al. and Kim et al. [6–8]. During start-up, hydrogen pushes oxygen, air, or possibly nitrogen that was introduced for purging water toward the outlet so that for a short time depending on various parameters like the flow rate and the channels geometry, a fraction of the anode compartment is filled with hydrogen while the other part is still occupied by the gas initially present. A potential appears at the inlet of the anode but not at the outlet, which generates internal currents under open-circuit conditions. Although these internal currents are scarcely studied, they were modeled by some authors [9–11] and they can be measured using segmented cells [12,13]. According to Meyer

and Darling [10] internal currents can be at the origin of fuel cell performance decay by creating abnormally high potentials at the cathode, causing carbon corrosion. Starting from experimental data measured thanks to a segmented cell, Siroma et al. [12] suggested that the double layer capacitance could play a major role in the origin of reverse currents and high potentials. In the following section, we present a segmented cell which was designed specifically for the study of internal currents: a particular attention was given to the current collection in order to reduce as much as possible all parasitic (contact and connecting) resistances. Data measured in various operating conditions are presented in the third section. They are used to validate a model based on capacitive effects which is described in the last section.

## 2. Experimental setup

The first segmented cell that was designed in our group in 2007 [13] allowed some observations of internal currents. Its performances were quite lower than those of usual fuel cells because of the large high frequency resistance entailed by the small surface devoted to current collection. Since, a new segmented cell with better performances was designed and built in order to obtain a good assessment of the magnitude of the internal currents (Fig. 1). Air and hydrogen flow through five 30 cm parallel straight channels of  $0.7 \text{ mm} \times 1 \text{ mm}$  in section. On the anode side, the channels are machined in an aluminum plate that is then gold plated. The cathode plate is in polycarbonate (transparent but non conductive) and the channel ribs are made of 15 mm long, 1 mm thick gold plated brass strips. They are inserted only between two adjacent channels so that  $4 \times 20 = 80$  strips were necessary for the five channels. Each

\* Corresponding author. Tel.: +33 0 3 83 59 55 48; fax: +33 0 3 83 59 55 51.  
E-mail address: [gael.maranzana@ensem.inpl-nancy.fr](mailto:gael.maranzana@ensem.inpl-nancy.fr) (G. Maranzana).

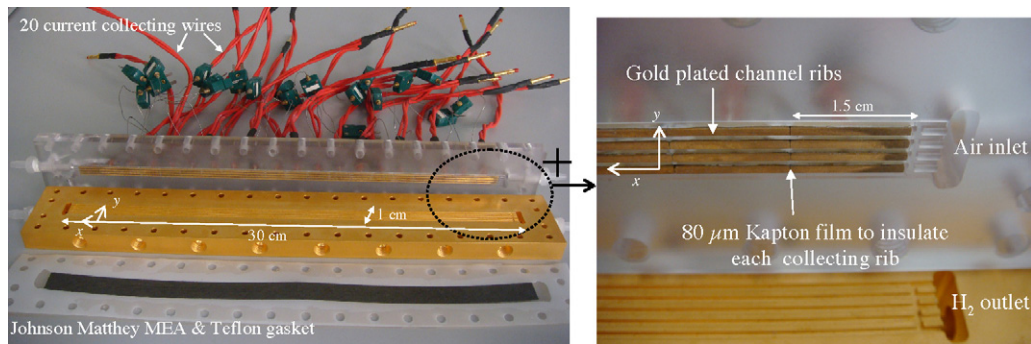


Fig. 1. View of the dismantled segmented cell and zoom on the segmented channel ribs.

strip is electrically isolated from the preceding and following ones (along the  $x$  axis in Fig. 1) thanks to a small  $2.3 \text{ mm} \times 1 \text{ mm}$ ,  $80 \mu\text{m}$  thick Kapton sheet. The main technical difficulty was to obtain a flat contact surface in order to make the contact resistance between the channel ribs and the backing layer as much uniform as possible. This was done by surfacing the channel ribs once they were embedded in the polycarbonate plate. They were then gold plated in a second step. The MEA (Johnson-Matthey) consists of a  $30 \mu\text{m}$  thick Nafion 212 membrane and of catalytic layers with an average Pt loading of  $0.4 \text{ mg cm}^{-2}$  at the anode and cathode. The active area is  $A = 30 \text{ cm}^2$ . The GDL is a  $190 \mu\text{m}$  thick carbon fibre paper (Toray TGP-H-060). The MEA is not segmented. For these experiments, the four adjacent strips are electrically connected outside the cell, which is equivalent to averaging the current intensity along the  $y$  direction. Thus, 20 wires (one per segment) drive the current toward 20,  $5 \text{ m}\Omega$  shunt resistors, which voltage drops allow an indirect measurement of the current intensity. Then, all segments are set to the same potential, as shown in the sketch of Fig. 2. The total resistance between the channel ribs and the point where the 20 segments are connected is about  $12 \text{ m}\Omega$ . The resistance between two consecutive brass strips being of  $175 \text{ m}\Omega$ , it is reasonable to assume that most of the current produced in a segment actually flows through the corresponding connecting wire instead of the GDL thickness according the plane direction. Numerical data (local current intensities and voltage) are recorded at a frequency of  $200 \text{ Hz}$  and with a 16-bit resolution thanks to a National Instrument SCXI multiplexer.

### 3. Experimental results

Several start-up experiments were performed with different values of the hydrogen flow rate, the anode compartment being initially filled with air or nitrogen. Nitrogen was used to study the effect of a purge after shut-down. The fuel cell was at ambient temperature ( $22^\circ\text{C}$ ) and air and hydrogen were humidified

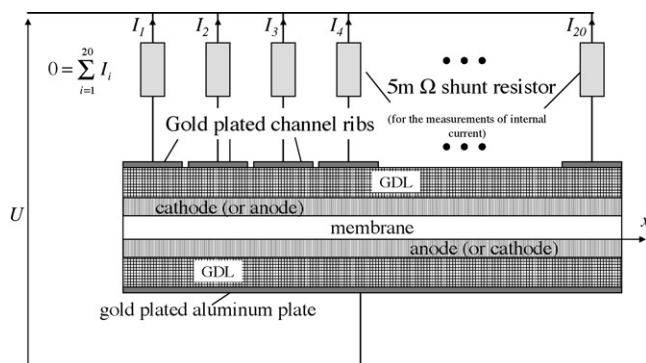


Fig. 2. Scheme of the electrical connections.

until saturation using bubblers (also at ambient temperature). The occurrence of internal currents can be seen in Fig. 3 with the simultaneous rise of the open circuit potential as functions of time. The hydrogen flow was set to  $3 \text{ cm s}^{-1}$  and  $1 \text{ m s}^{-1}$ , which correspond to theoretical values of the current density in steady state of  $0.03$  and  $1 \text{ A cm}^{-2}$  (with a stoichiometry of 1). The air flow was set to  $5 \text{ m s}^{-1}$ , which corresponds to a steady state current density of  $1 \text{ A cm}^{-2}$  with a stoichiometry of 2.

The sum of the currents flowing through the 20 segments being null at open circuit, the current that is produced by the first segment is necessarily distributed between the others. Thus, when hydrogen reaches the inlet of the cell the electrical current produced by the first segment flows toward the 19 others so that reverse currents (by reference to the normal fuel cell operation) can be measured. The current produced by the first segment reaches a maximum and then decreases while the hydrogen front is moving forward. Similar current profiles are observed in the other segments but with a lower intensity. Once the hydrogen front has reached the anode outlet, the cell voltage is close to the open circuit voltage and the internal currents have almost entirely disappeared. Their intensity increases with the incoming hydrogen velocity until about  $1 \text{ m s}^{-1}$ ; then, it remains constant whatever the hydrogen velocity, probably because of some imperfections in the experimental setup affecting the time constant of the hydrogen flow. With this fuel cell and in the range of operating conditions we have tested, it can reach a maximum of  $1 \text{ A cm}^{-2}$  for positive currents and  $0.25 \text{ A cm}^{-2}$  for negative currents.

#### 3.1. Effect of the initial gas that filled the anode

The phenomena observed when the gas initially present in the anode compartment is nitrogen or air differ in two points. First, for the lower hydrogen flow rates, the intensity of internal currents is more important with air. The difference is here of the order of  $0.2 \text{ A cm}^{-2}$ , which cannot be explained by carbon oxidation at the cathode as described in [9–11]: current densities corresponding to carbon oxidation must be of a few  $\text{mA cm}^{-2}$  [10] only. A more probable explanation is that the direct oxidation of some hydrogen and oxygen on platinum at the anode improves the hydration of the MEA and raises the local temperature which in turn increases the intensity of internal currents. For the higher hydrogen flow rates, the intensity of internal currents is identical whatever gas is in the anode compartment. This convergence of the magnitude of the internal currents with the hydrogen velocity could be explained either by the imperfections of the experimental setup or by a less significant effect of the MEA hydration mentioned above.

The other main difference between air and nitrogen lies in the peak of current density, which happens earlier with nitrogen. Globally, the fuel cell voltage rises also faster with nitrogen. This effect is most probably also linked with the direct oxidation of hydrogen

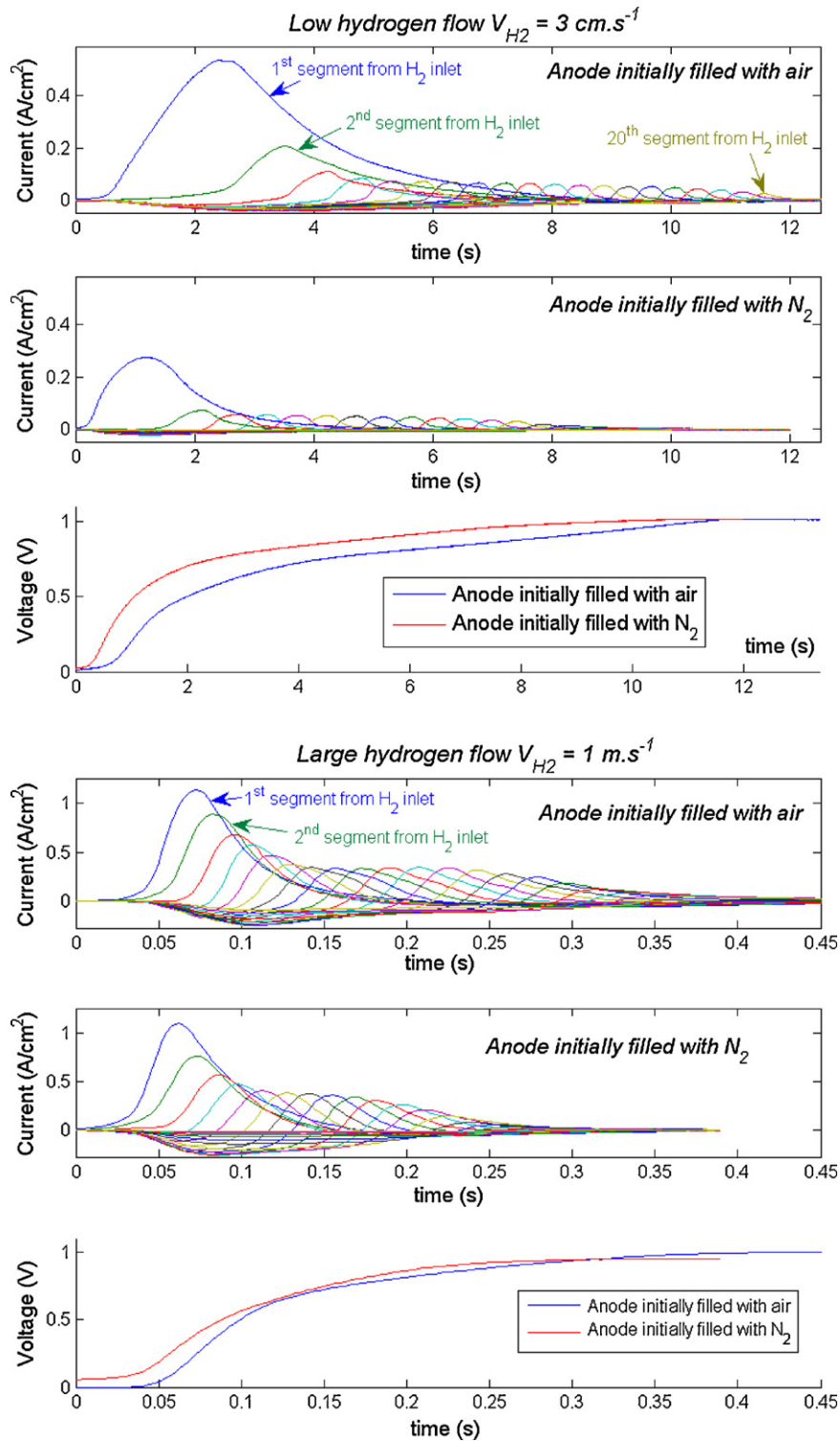


Fig. 3. Internal currents and open circuit potential as function of time for two different hydrogen inlet flows and for anode initially filled with air or nitrogen.  $T = 22^\circ\text{C}$ . Saturated air and hydrogen at the cathode and anode.

in the presence of oxygen, which slows down the velocity of the hydrogen front in the anode compartment.

#### 4. Modelling

The model presented in the following demonstrates that the occurrence of internal currents can be explained mostly by capacitive effects. Carbon oxidation and other redox mechanisms are

considered only via a leakage resistance: redox potentials other than the oxidation of hydrogen are neglected. In order to focus on the main phenomena, the gas initially present in the anode compartment is nitrogen. The case of oxygen is not considered.

For the sake of simplicity, the electrical behaviour of the cell is partially linearized. The basic building block of the model is a generic equivalent circuit of the electrodes which is assumed to be valid whatever the direction of the electrical current (Fig. 4). The

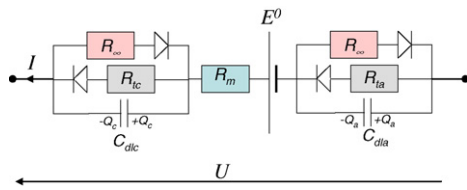


Fig. 4. Electrical model of a MEA segment.

electrodes are represented by a double layer capacitance  $C_{dl}$  in parallel with a charge transfer resistance  $R_{tc}$  and a leakage resistance  $R_{\infty}$  that accounts for the oxidation of carbon and/or other possible redox phenomena. It is assumed that the value of  $R_{tc}$  becomes infinite for negative currents (from anode to cathode) because the voltage maximum value reached during start-up does not allow the electrolysis of water. Moreover, the leakage resistance  $R_{\infty}$  is neglected when a faradic current exists ( $Q_{a,c} > 0$ ): it becomes also infinite. In Fig. 4, the diodes in series with  $R_{tc}$  and  $R_{\infty}$  control their values as functions of the direction of the electrical current. The resistance of the electrolyte and the various contact resistances are accounted for through a single high frequency resistance  $R_m$  in series with the anode and the cathode (Fig. 5).

The electrodes as represented in Fig. 4 operate following three modes:

- Without hydrogen in the anode compartment, the direction of the electrical current is negative. It flows through the leakage resistance  $R_{\infty}$  and through the capacitances  $C_{dlc}$  and  $C_{dla}$  which charge progressively ( $Q_c, Q_a < 0$ ) as the electrical current decreases (in absolute value).
- When hydrogen comes in the anode compartment, a voltage  $E^0$  appears between the electrodes and adds to the voltage across of the two partially charged capacitances. The electric current  $I^k$  becomes positive and the double layer capacitances  $C_{dlc}$  and  $C_{dla}$  discharge.
- When the charge of the capacitances becomes null (i.e. when the fuel cell voltage is equal to  $E^0$  or lower) the electrical current  $I^k$  becomes a faradic current and it flows through the charge transfer resistances  $R_{tc}$  and  $R_{ta}$ .

The channel is discretized into  $n$  segments (Fig. 5) from the inlet (no. 1) to the outlet (no.  $n$ ). The geometry of the channel and the velocity of hydrogen define a convection time  $tc_k$  at which the  $k$ th segment is occupied by hydrogen whereas only nitrogen is present at  $t < tc_k$ . Air is assumed to be always present in enough quantity in the cathode compartment.

The global equivalent electrical circuit of the fuel cell leads to a system of  $3n + 1$  ordinary differential equations with  $3n + 1$  unknowns. The unknowns are the potential difference between cathode and anode  $U$ , the current intensity  $I^k_{1 \leq k \leq n}$  through the  $n$  segments, the charge of the  $n$  cathode capacitances  $Q_c^k_{1 \leq k \leq n}$  and the charge of the  $n$  anode capacitances  $Q_a^k_{1 \leq k \leq n}$ :

$$\begin{cases} U = E^k - R_m I^k - \frac{Q_c^k}{C_{dlc}^k} - \frac{Q_a^k}{C_{dla}^k} & (E^k = 0 \text{ if } k > i)_{1 \leq k \leq n} \\ I^k = \frac{dQ_c^k}{dt} + \frac{Q_c^k}{R_{tc}^k C_{dlc}^k} = \frac{dQ_a^k}{dt} + \frac{Q_a^k}{R_{ta}^k C_{dla}^k} & (R_{ta}^k = R_{\infty} \text{ if } Q_a^k < 0)_{1 \leq k \leq n} \\ 0 = \sum_{i=1}^n I^i \end{cases}$$

where  $E^k$  stands for the open circuit voltage (in steady state).  $E^k = 0$  if  $k > i$  and  $E^k = E_0$  if  $k \leq i$ . Replacing  $I^k$  by its expression (the second equation) in the first and third equations and considering that  $U$  is constant in all the segments makes it possible to reduce the dimension of the system to  $2n$ :

$$\frac{d}{dt} \mathbf{Q} = \mathbf{M}(t) \mathbf{Q} + \mathbf{S}(t) \quad \mathbf{Q} = (Q_c^1 \dots Q_c^n \quad Q_a^1 \dots Q_a^n)^t$$

where the remaining unknowns are the charges of the capacitances.  $\mathbf{M}$  is a  $2n \times 2n$  square matrix that is time dependent. The source term  $\mathbf{S}$  is also time dependent. This system can be easily solved by a Runge-Kutta method but an iterative loop must be used to adjust the location of the hydrogen front by subtracting the consumed quantity – derived from the Faradic current – from the total quantity of hydrogen injected. Actually, except in the case of very low hydrogen flow rates, the velocity of the front remains almost constant due to the very low hydrogen consumption. Note that the number of segments used for the simulations ( $n=200$ ) is much

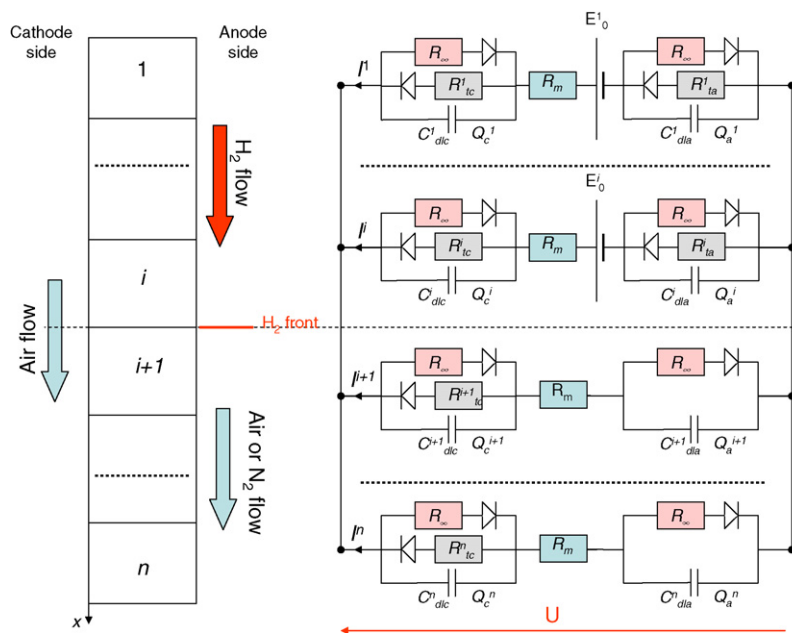


Fig. 5. Global equivalent electrical circuit of the fuel cell at time  $t < tc_{i+1}$ . The charge transfer resistance  $R_{tc}$  at the anode is not represented in the absence of hydrogen because it has no physical meaning.

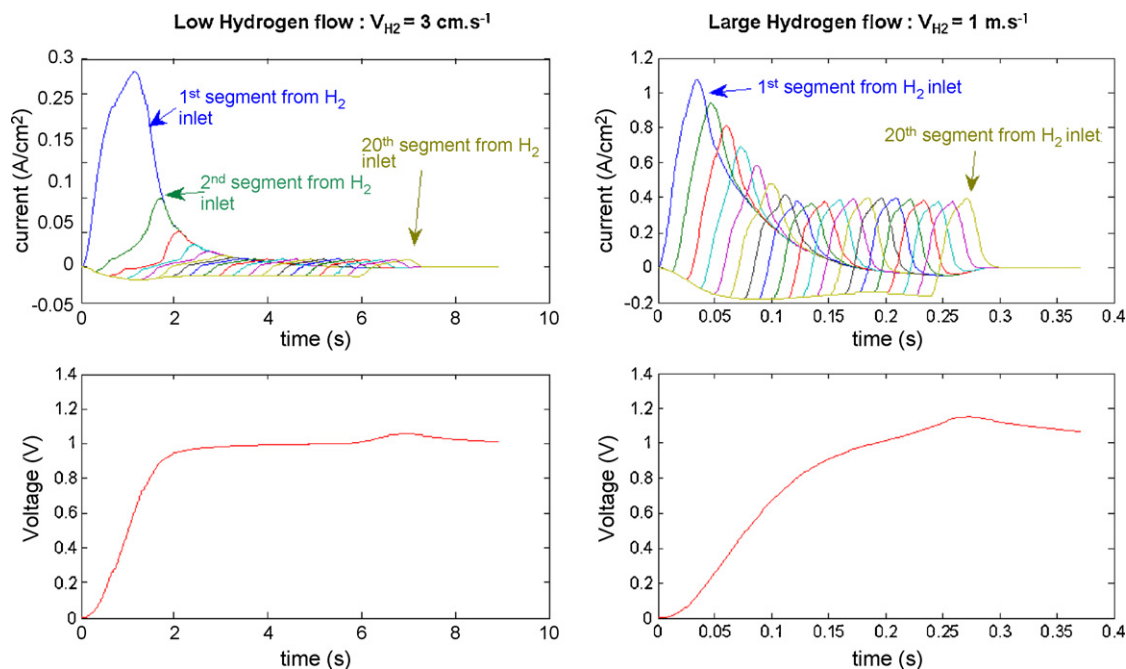


Fig. 6. Numerical results obtained with  $E_0 = 1$  V,  $R_m = 0.4 \Omega \text{ cm}^2$ ,  $C_{dla} = C_{dlc} = 0.02 \text{ F cm}^{-2}$ ,  $R_\infty = 1 \Omega \text{ cm}^2$ ,  $R_{tc} = 0.2 \Omega \text{ cm}^2$  and  $R_{ta} = 0.05 \Omega \text{ cm}^2$ .

higher than the number of segments in the experimental cell: the numerical results presented below are averaged over 10 consecutive segments. In order to avoid numerical instabilities, it was found convenient to increase linearly  $E^k$  with time in the  $k$ th segment when  $t_{ck} < t < t_{ck+1}$ .

#### 4.1. Parameters setting

The model is governed by seven parameters: the charge transfer resistances  $R_{ta}$  and  $R_{tc}$ , the double layer capacitances  $C_{dla}$  and  $C_{dlc}$ , the high frequency resistance  $R_m$ , the leakage resistance  $R_\infty$  and the open circuit potential in fuel cell mode  $E_0$ .  $E_0$  is set to 1 V, which is close to the actual values. The high frequency resistance is set to the experimental value measured at 1000 Hz:  $R_m = 0.4 \Omega \text{ cm}^2$ . The double layer capacitances are highly linked to the potential: the retained values  $C_{dla} = C_{dlc} = 0.02 \text{ F cm}^{-2}$  corresponds to experimental results (for the cathode) measured by impedance spectroscopy at 0.7 V. The charge transfer resistances depend on the faradic current but they were adjusted to obtain the right order of magnitude of the internal currents:  $R_{tc} = 0.2$  and  $R_{ta} = 0.05 \Omega \text{ cm}^2$ . The leakage resistance is of course also highly non-linear and it was adjusted in order to obtain realistic voltage profiles:  $R_\infty = 1 \Omega \text{ cm}^2$ . With an infinite leakage resistance, the fuel cell voltage would reach values close to 2 V resulting from the sum of the open circuit voltage and of the voltage of the anode and cathode double layer capacitances, which can be charged up to +1 V while air is still present in the last part of the anode compartment. However, in any case, the steady state fuel cell voltage is always equal to  $E_0 = 1$  V once the double layer capacitances have discharged through the leakage resistances.

#### 4.2. Numerical results

Fig. 6 presents the evolution with time of the internal currents and of the fuel cell voltage as determined by the model with the values of the parameters stated above. The hydrogen flow rate was adjusted so that the inlet velocity corresponds to the experimental values in Fig. 3 ( $3 \text{ cm s}^{-1}$  and  $1 \text{ m s}^{-1}$ ). The experimental (Fig. 3) and numerical results (Fig. 5) are close to each other, at least in

qualitative terms. Of course, using constant values for the double layer capacitances, the charge transfer resistances and the leakage resistance is a strong assumption but the model shows that the dominant phenomena are probably linked with the double layer capacitances. Carbon oxidation should occur simultaneously but its contribution to the internal currents is by all appearances negligible.

One can also notice that the model predicts a transient voltage rise over the steady state open circuit voltage ( $E_0 = 1$  V). This voltage rise can be observed experimentally shortly after fuel cell start-up: according to these numerical results, it can be explained only to 2D and capacitive effects. However, other phenomena can show similar effects, like hydrogen crossover through the membrane for instance.

## 5. Conclusion

The internal currents that occur during PEMFC start-up have been measured using a segmented cell which performances are equivalent to those of usual commercial cells. Experiments show that the transient current densities can reach up to  $1 \text{ A cm}^{-2}$ . This is far more important than the expected order of magnitude of the current densities associated with carbon oxidation, which is only of a few  $\text{mA cm}^{-2}$ . The predominant phenomenon that explains the internal currents is the charge and discharge of the double layer capacitances. A simple model with constant values of the electric parameters yields numerical results close to the experimental ones. It also explains the transient voltage rise (over the steady state open circuit voltage) that is sometimes observed experimentally shortly after the fuel cell start-up. In the near future, this model will be used to estimate the rate of carbon oxidation along the cell as a function of the hydrogen velocity. In parallel, the local ageing of the electrodes will be characterized experimentally after subjecting the fuel cell to start-up and shut-down cycles.

## Acknowledgements

The authors would like to express their gratitude to those who made this work possible, the technical team: Jean-Yves

Morel, Christophe Gigant, Denis Lallement, Michel Marchand, Pascal Thomann and Salomon's Jewellery.

## References

- [1] Y. Shao, G. Yin, Y. Gao, J. Power Sources 171 (2007) 558–566.
- [2] S.D. Knights, K.M. Colbow, J. St-Pierre, D.P. Wilkinson, J. Power Sources 127 (2004) 127–134.
- [3] J. St-Pierre, D.P. Wilkinson, S. Knights, M.L. Bos, J. New Mater. Electrochem. Syst. 3 (2000) 99–106.
- [4] P. Yu, M. Pemberton, P. Plasse, J. Power Sources 144 (2005) 11–20.
- [5] T. Akita, A. Taniguchi, J. Maekawa, Z. Siroma, K. Tanaka, M. Kohyama, K. Yasuda, J. Power Sources 159 (2006) 461–467.
- [6] H. Tang, Z. Qi, M. Ramani, J.F. Elter, J. Power Sources 158 (2006) 1306–1312.
- [7] Q. Shen, M. Hou, D. Liang, Z. Zhou, X. Li, Z. Shao, B. Yi, J. Power Sources 189 (2009) 1114–1119.
- [8] J. Kim, J. Lee, Y. Tak, J. Power Sources 192 (2009) 674–678.
- [9] C.A. Reiser, L. Bregoli, T.W. Paterson, J.S. Yi, J.D. Yang, M.L. Perry, T.D. Jarvi, Electrochem. Solid-State Lett. 8 (6) (2005) A273–A276.
- [10] J.P. Meyers, R. Darling, J. Electrochem. Soc. 153 (8) (2006) A1432–A1442.
- [11] N. Takeuchi, T.F. Fuller, J. Electrochem. Soc. 155 (7) (2008) B770–B775.
- [12] Z. Siroma, N. Fujiwara, T. Ioroi, S. Yamazaki, H. Senoh, K. Yasuda, K. Tanimoto, J. Power Sources 172 (2007) 155–162.
- [13] G. Maranzana, O. Lottin, T. Colinart, S. Chupin, S. Didierjean, J. Power Sources 180 (2008) 748–754.